Hindawi
Journal of Chemistry
Volume 2018, Article ID 4319149, 11 pages
https://doi.org/10.1155/2018/4319149

Research Article

Preparation of Microporous Carbon from *Sargassum horneri* by Hydrothermal Carbonization and KOH Activation for CO_2 Capture

Ganning Zeng,[1,2] Sa Lou,[3,4,5] Huijuan Ying,[3,4,5] Xi Wu,[3] Xin Dou,[3] Ning Ai,[3,4,5] and Jiawei Wang[6]

[1]*Ocean College, Zhejiang University of Technology, Hangzhou 310014, China*
[2]*Northern Region Persistent Organic Pollution Control (NRPOP) Laboratory, Engineering and Applied Science, Memorial University of Newfoundland, St. John's, NL, Canada A1B 1X5*
[3]*College of Chemical Engineering, Zhejiang University of Technology, Hangzhou 310014, China*
[4]*Zhejiang Province Key Laboratory of Biomass Fuel, Hangzhou 310014, China*
[5]*Biodiesel Laboratory of China Petroleum and Chemical Industry Federation, Hangzhou 310014, China*
[6]*Chemical Engineering and Applied Chemistry, Aston University, Aston Triangle, Birmingham B4 7ET, UK*

Correspondence should be addressed to Ning Ai; aining@tsinghua.org.cn

Received 4 August 2018; Revised 4 October 2018; Accepted 12 November 2018; Published 13 December 2018

Academic Editor: Ana B. Martin-Diana

High-performance microporous activated carbon (AHC) for CO_2 capture was prepared from an emerging marine pollutant, *Sargassum horneri*, via hydrothermal carbonization (HTC) and KOH activation. The as-synthesized carbon material was characterized by N_2 sorption-desorption measurement, TGA, SEM, XRD, FTIR, and elemental analysis. Impressively, the activated carbon exhibited high specific surface area (1221 m^2/g), narrow distributed micropores (~0.50 nm), and a relatively high nitrogen content (3.56 wt.%), which endowed this carbon material high CO_2 uptake of 101.7 mg/g at 30°C and 1 bar. Moreover, the carbon material showed highly stable CO_2 adsorption capacity and easy regeneration over four adsorption-desorption cycles. Two kinetic models were employed in this work and found that the pseudo-first-order kinetic model (R^2 = 0.99) provided the best description. In addition, the high CO_2 uptake is mainly attributed to the presence of abundant narrow microporous. The macroporous structure of hydrochar (HC) played an important role in the production of microporous carbon with high adsorption properties. This work provides an efficient strategy for preparing microporous activated carbon from *Sargassum horneri*, and AHC is a promising candidate acting as an efficient CO_2 adsorbent for further industrial application.

1. Introduction

Diverse groups of organisms are found living in the ocean, of which, macroalgae is at least 10,000 different species described to date. Currently, the production of high value-added chemicals from macroalgae has been considered as a promising and long-term methodology to meet the word energy demands, reduce the global warming, alleviate food shortage, etc. [1–3]. *Sargassum horneri* (*S. horneri*) is one of the common macroalgae, and it is artificially cultivated for aquatic eutrophication restoration due to its superior absorption capability of nutrients. Meanwhile, *S. horneri* can compete with microplankton, protozoan, and even bacteria for nutrients, inhibiting the harmful algae blooms [4]. However, ocean-scale build-up of *S. horneri* blooms broke out unprecedentedly, leading to the occurrence of massive golden tides along the West African coast in spring, 2011 [5]. Outbreak of golden tides caused by *S. horneri* was also found in the Yellow Sea of China in December 2016, causing serious economic loss (more than U.S. $73 million) [6]. Moreover, the so-called *S. horneri* golden tides brought its detrimental side to tourism-based economics, coastal ecosystems, ocean transportation, and water quality [5, 6]. Thus, it is necessary to utilize this emerging abundant waste effectively.

The macroalgae has been widely used to absorb heavy metals and organics or produce bioactive compounds and hydrocolloids [7–10]. *S. horneri* is a prolific renewable

carbon source, and its cell walls are primarily composed of fibrous cellulose network and alginate mucilage [11–13]. The alginate polymers enable the absorption of metal cations (i.e., Ni^{2+}, Fe^{3+}, and Mg^{2+}) to form metal alginates (M-alginates). After carbonization of the M-alginates and subsequent acid washing, the metal cations can be removed to produce carbon materials with special porous structure [12]. Therefore, it is promising to utilize *S. horneri* as a precursor for the production of carbon materials.

Pyrolysis is a common method for converting biomass into carbon. However, traditional dry pyrolysis cannot meet the requirement for high carbon yield [14, 15]. Hydrothermal carbonization (HTC) is a thermochemical conversion process where an organic substrate is converted into a solid product enriched in carbon content in the presence of water [16]. It was first described in 1913 by Bergius and was reintroduced to the public in the 21st century by Titirici and Antonietti in Germany [17]. In the recent years, HTC has been discovered to be a very effective and advantageous synthesis method for converting biomass into carbon materials, which are referred as hydrochars. However, hydrochar obtained by the sole HTC process exhibits low porosity, which hinders its potential application for catalysis, electrochemistry, and sorption. From this view of point, further activation treatment is considered as an effective strategy to introduce porosity. In general, activated carbons with well-developed porosity, especially narrow microporosity, are prepared by chemical activation using activating agents such as KOH, $ZnCl_2$, and H_3PO_4 [18]. Recently, activated carbons especially microporous carbon prepared by KOH activation have emerged as the most promising adsorbent for CO_2 capture due to their low cost of preparation, high specific surface area, and excellent chemical stability [13, 19].

In terms of the CO_2 capture by activated carbons, it has been reported that the narrow micropores play a decisive role in CO_2 adsorption capacity [20–23]. This is due to the fact that the interaction energy of CO_2 molecules and adsorbent can be greatly enhanced due to the overlapping of the potential fields from the adjacent walls when the adsorption occurs in narrow micropores [21, 24]. This strong adsorption potentials generated by narrow micropores can enhance their filling by the CO_2 molecules. Recently, Sevilla et al. reported that CO_2 uptake capacity was mainly determined by the volume of small micropores (<1 nm) [20, 21]. Further research indicated that the micropores with a diameter smaller than 0.8 nm played a key role in determining CO_2 capture on N-free carbide-derived carbons at 1 bar [22]. Zhang et al. pointed out that the CO_2 capture capacity strongly depended on the small micropores (<0.54 nm) under different adsorption conditions [23]. Therefore, the critical target is to generate narrow micropores for achieving highly efficient CO_2 capture. In addition, it is generally accepted that the introduction of nitrogen-containing functional groups into carbon materials can generate more active sites, strengthening the interactions between carbon surface and CO_2 molecules for improving the CO_2 adsorption capacity [25]. The interactions are associated with the formation of the Lewis basic sites and the hydrogen-bonding between carbon surface and CO_2 molecules [26, 27].

Previous research studies focused on the utilization of macroalgae to synthesize carbon materials applied in fields such as catalysts, supercapacitors, and lithium-sulfur batteries [28–34]. However, to the best of our knowledge, the study on preparing microporous carbon from macroalgae for CO_2 uptake was seldom reported. In this work, we reported a facile method to synthesis microporous activated carbon with large quantities of narrow micropores (~0.50 nm). The synthesis was performed under mild hydrothermal conditions and subsequent KOH activation, and the product was applied for carbon capture and storage (CCS). The CO_2 capture capacity, kinetics, and regeneration of microporous carbon were investigated.

2. Materials and Methods

2.1. Materials. *Sargassum horneri* was sampled from the Wenzhou coastal area, Zhejiang province, P.R China. *S. horneri* was washed with deionized water, then crushed by grinder, and sieved into a particle size in the range of 106–180 μm. Ammonium iron (II) sulfate hexahydrate (Fe $(NH_4)_2(SO_4)_2{\cdot}6H_2O$, 99.5%, A.R.), potassium hydroxide (KOH, A.R.), and hydrochloric acid (HCl, 38%, A.R.) were purchased from Sinopharm Ltd. (China). N_2 and CO_2 (99.99%) gases were purchased from Hangzhou Special Gas Co., ltd.

2.2. Preparation of Microporous Carbon. The preparation of hydrochar was done according to our previous work [35, 36], i.e., 1.96 g $Fe(NH_4)_2(SO_4)_2{\cdot}6H_2O$, 10.0 g *S. horneri*, and 40 mL distilled water were mixed and sealed in 75 mL stainless steel autoclave. Then, the autoclaved mixture was transferred to a preheated oven and hydrothermally treated at 180°C for 2 h. After cooling to room temperature, the obtained solid product, denoted as hydrochar (HC), was washed with distilled water until neutral pH and dried at 100°C overnight. Then, the HC was activated with KOH as follows: the equivalent mass of HC and KOH was mixed and then heated in the tube furnace at 600°C for 2 h under N_2 atmosphere at a heating rate of 10°C·min^{-1}. The resulting solid product was washed with 1 M HCl to remove inorganic salts, washed thoroughly with distilled water until neutral pH, and subsequently dried at 100°C overnight. Activated HC product is denoted as AHC. The AHC was stored in a desiccator for further characterizations.

2.3. Characterization. The surface morphology of the microporous carbon was characterized with a Hitachi S-4700 scanning electron microscope (SEM) at 5.0 kV and 15.0 kV.

Nitrogen adsorption-desorption isotherms were measured at 77 K using an automatic surface area and a pore size analyzer (3H-2000PS1), and the CO_2 adsorption experiment was performed at 273 K. Prior to sorption measurements, the samples were degassed at 200°C for 3 h. BET surface area and pore volume were determined by N_2 adsorption-desorption isotherms. The specific surface area was calculated using the Brunauer–Emmet–Teller (BET) method at relative pressure (P/P_0) values ranging from 0.04 to 0.32; the total pore volume

(V_t) was determined by adsorption amount at the relative pressure of 0.99; the micropore surface area (S_{micro}) and micropore volume (V_{micro}) were calculated by the t-plot analysis; the pore size distributions (PSD) were obtained using the density functional theory (DFT) method.

The infrared spectra of the samples were acquired using a Nicolet 6700 FTIR spectrometer by averaging 24 scans in the 4000–400 cm^{-1} spectral range at 4 cm^{-1} resolution, and a KBr pellet was used as a reference sample.

The XRD patterns were collected using a PANalytical X'Pert PRO diffractometer with a Cu-Kα radiation (40 kV, 40 mA).

Elemental analysis was carried out on an elemental analyzer (Elementar Vario MACRO cube, Germany), and oxygen content was determined by difference.

The thermogravimetric analysis (TGA), derivative thermogravimetry (DTG), and CO_2 adsorption experiments were performed on a thermogravimetric analyzer (NETZSCH TG 209 F3 Tarsus, Germany).

2.4. CO_2 Adsorption Experiments. The CO_2 adsorption performance of the carbon samples were measured by a thermogravimetric analyzer. Initially, 10 mg of the sample was placed in an alumina crucible loaded in a TGA furnace. Prior to each adsorption experiment, the carbon was heated up to 120°C (10°C/min) and kept for 30 min to remove moisture under N_2 flow (40 mL·min^{-1}). Then, the carbon sample was cooled to desired adsorption temperature, i.e., 30, 45, and 60°C, respectively, under which the CO_2 adsorption studies were performed for 90 min at a rate of 50 mL·min^{-1}. Moreover, the adsorbent regeneration was done by heating to 120°C for 30 min at 10°C·min^{-1} under N_2 flow (40 mL·min^{-1}). To check the adsorbent stability, the adsorption/desorption procedure was repeated 4 times.

2.5. Experimental Description. HC was prepared from *S. horneri* by hydrothermal treatment in our previous work [35, 36]. During the hydrothermal carbonization, we investigated the effects of the reaction temperature, the reaction time, and the mass ratio of *S. horneri* to deionized water on the carbon yield. Fe $(NH_4)_2(SO_4)_2{\cdot}6H_2O$ was used as the catalyst because (i) the presence of iron ions could effectively speed up the hydrothermal carbonization process and significantly reduce the reaction time and the reaction temperature [37, 38], (ii) iron ion had a catalytic effect on the evolution of gases, contributing to produce the carbon materials with higher porosity and surface area in the HTC process [39], and (iii) the introduction of the N-containing surface groups could enhance the CO_2 adsorption capacity. Finally, the carbon recovery and yield could reach up to 65.0% and 51.4%, respectively. The optimized conditions could be described as follows: the reaction temperature at 180°C, the reaction time for 2 h, and the mass ratio of *S. horneri* to deionized water is 10/40.

3. Results and Discussion

3.1. Thermogravimetric Analysis. To investigate the thermal decomposition of *S. horneri*, hydrochar (HC) and the mixture of HC and KOH (HC-KOH), the TGA and DTG analysis was conducted under nitrogen atmosphere, as shown in Figure 1. Three stages of weight loss in the TGA-DTG curve of *S. horneri* have been observed in Figure 1(a). The first stage occurred at the temperature range of 30–200°C, with one peak centered at 68°C, due to vaporization of adsorbed water on the surface [40]. In the second stage, a significant weight loss of approximately 38% was achieved between 200 and 400°C, corresponding to the decomposition of biopolymer fractions [41]. In the DTG curve, two extensive peaks were detected between 200 and 350°C. The first peak (between 200 and 280°C) and the second peak below 350°C might be associated with the decomposition of carbohydrates and proteins, respectively. The thermal degradation patterns were similar to that of macroalgae reported by Li et al. [42]. The weight loss of the final stage at a temperature range of 400–800°C might be attributed to the degradation of lignin and remaining proteins [43]. In the case of HC, the major weight loss occurred at a temperature range of 200–400°C, and only one sharp peak at 335°C was detected in Figure 1(b), indicating that the biopolymer fractions especially hemicellulose were decomposed after the hydrothermal carbonization. Similar phenomenon was also found in other studies [44]. For the mixture of HC and KOH, a total weight loss of 60% and three major stages in the thermal decomposition were found in Figure 1(c). The first stage mass loss from room temperature to 200°C was associated with the dehydration of KOH. The second stage in the wide temperature range of 200–600°C could be attributed to the decomposition of the biopolymer and KOH [45]. Besides, there is a significant weight loss in the final stage above 600°C, suggesting that the carbon is severely etched by KOH to form the well-developed porous structure [46].

3.2. Physical Properties of Activated Carbon. The morphologies of the *S. horneri*, HC, and AHC are shown in Figure 2. As shown in Figure 2(a), the surface of the *S. horneri* was smooth and exhibited a channel-like structure. After hydrothermal treatment, the surface of the HC became rough and showed an irregular and overlapping layered structure (Figure 2(b)). In addition, the HC surface also presented the cross-linked macropore structure which contributed to the diffusion of KOH. Moreover, the HC had good affinity to KOH solution due to its hydrophilic surface. After KOH activation, the original morphology of the HC was completely destroyed and transformed into honeycomb-like structures (Figure 2(c)). Obviously, neighboring pores were connected and distributed randomly in the AHC after the HTC and activation process (Figure 2(d)).

N_2 sorption-desorption isotherms and pore size distributions for *S. horneri*, HC, and AHC are described in Figure 3, and the corresponding physical properties are presented in Table 1. It can be seen from Table 1 that HC had a low BET surface area (26.64 $m^2{\cdot}g^{-1}$) and negligible micropore volume, corresponding to macropore porosity shown in Figure 2(b). This phenomenon was similar to hydrochar that originated from other biomass [34, 47, 48]. It is worth mentioning that the BET surface area of HC was

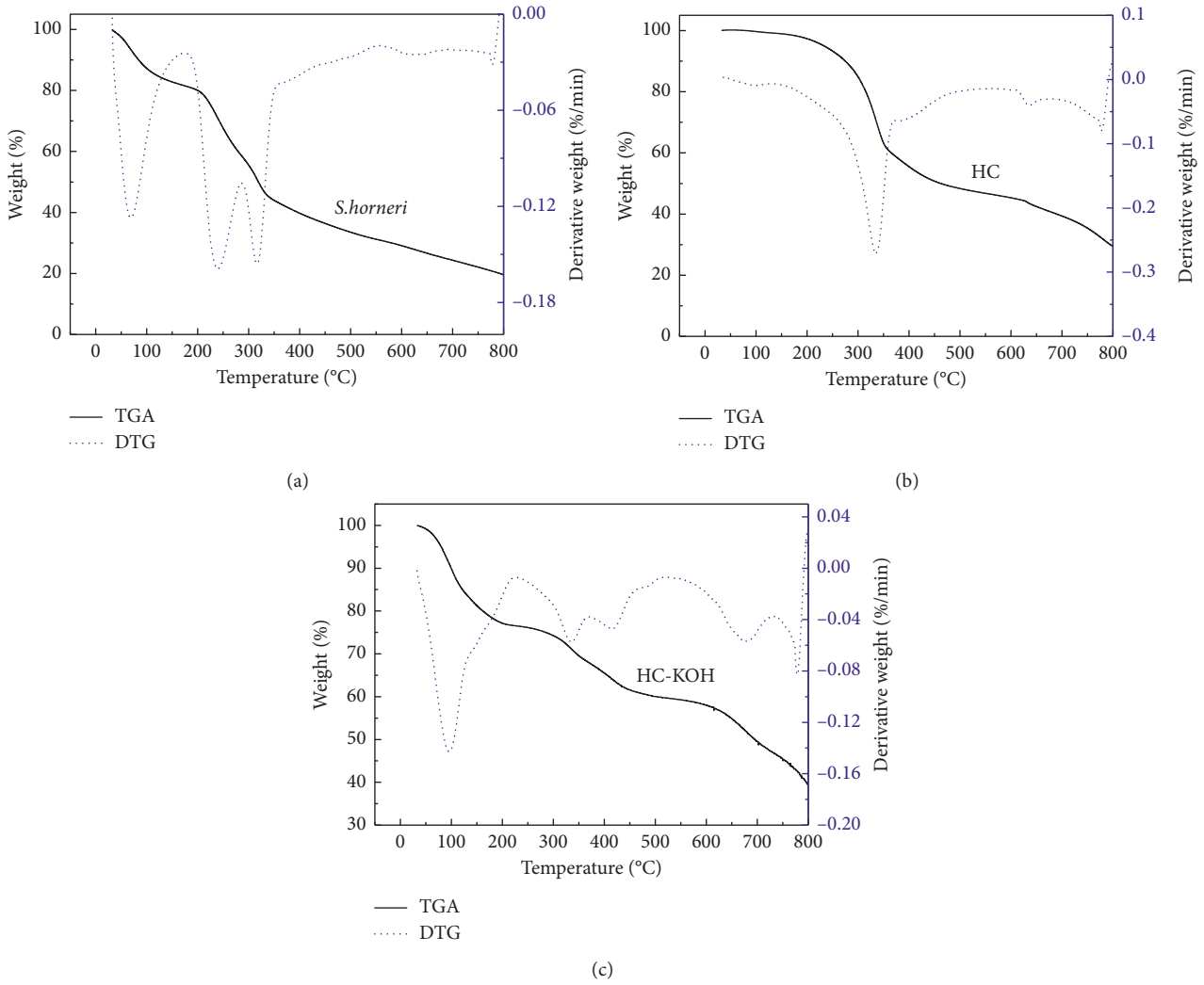

Figure 1: TGA and DTG curves for (a) *S. horneri*, (b) hydrochar (HC), and (c) the mixture of HC and KOH (HC-KOH) under N_2 flow.

higher than the hydrochars from other biomass such as *Enteromorpha prolifera* ($1.4\ m^2 \cdot g^{-1}$) [34], maize silage ($12\ m^2 \cdot g^{-1}$) [47], and pinewood ($21\ m^2 \cdot g^{-1}$) [48], probably due to the special structure of *S. horneri* and the addition of catalyst. In Figure 3(a), the HC exhibited a typical type III isotherm with a H3 hysteresis loop at relative pressure (P/P_0 = 0.5–1.0), corresponding to a mesoporous or macroporous structure with slit-like geometry, which is formed by the accumulation of flaky particles. AHC showed a standard type I isotherm and a steep increase in nitrogen uptakes at low relative pressure ($P/P_0 < 0.05$), indicating that KOH activation could promote the formation of abundant micropores in the carbon. To further investigate the porosity of the microporous carbon, the CO_2 adsorption experiment was carried out at 273 K. As shown in Figure 2(c), the pore size distribution showed that AHC possessed abundant narrow micropores (~0.50 nm). Cui et al. reported that the largest adsorption energy could be reached when the pore size of the adsorbent was 1–2 times larger than the kinetic diameter of the adsorbate molecule [49]. The kinetic diameter of CO_2 is 0.33 nm; hence, superior CO_2 adsorption capacity can be achieved by AHC with abundant narrow micropores of about 0.50 nm.

3.3. Chemical Properties of Activated Carbon. Elemental compositions of *S. horneri*, HC, and AHC are presented in Table 2. The hydrothermal carbonization of *S. horneri* significantly increased the relative carbon content from 41.25% to 52.77%. A van Krevelen diagram (in Figure 4) [50] was applied to analyze the reaction pathways of the carbonization process. The H/C atomic ratio decreased from 1.66 in the *S. horneri* to 1.13 in the HC, and the O/C atomic ratio descended from 0.89 to 0.54, indicating that the HTC process of *S. horneri* followed the pathways of dehydration and decarboxylation process [36]. After KOH activation, the relative carbon content of AHC increased from 52.77% to 71.40%, while the nitrogen content exhibited a small decrease, which might be related to the decomposition of unstable nitrogen-containing groups.

It has been proven that the CO_2 adsorption on activated carbon also depended on the surface functional groups. Therefore, the functional groups of HC and AHC were analyzed using FTIR spectroscopy as shown in Figure 5. For the HC, the adsorption peak in the 3000–3500 cm^{-1} range was associated with H-bonded O-H vibration [51], and the band at around 2930 cm^{-1} was assigned to C-H stretching.

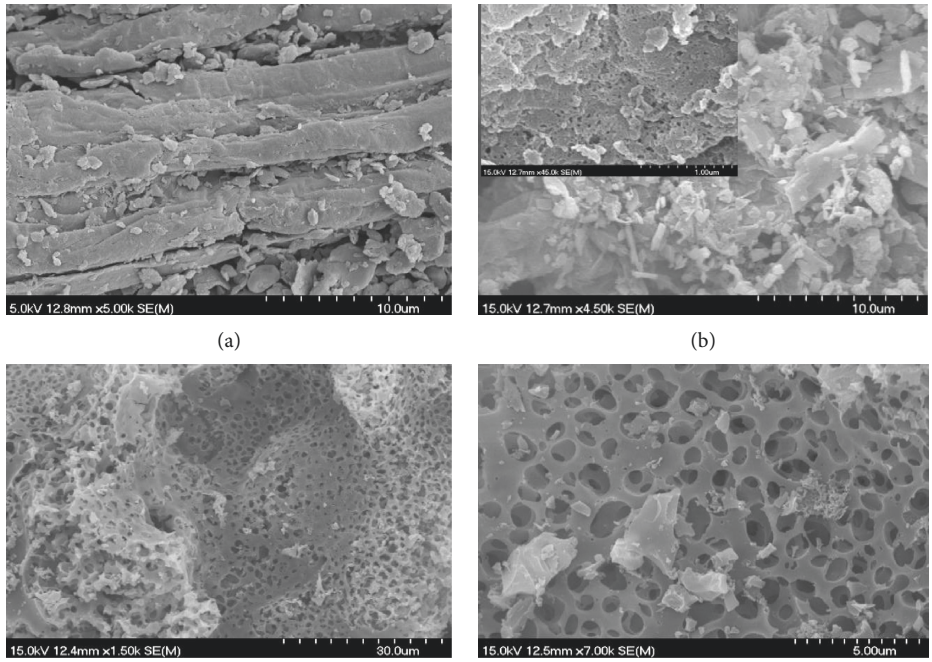

Figure 2: SEM images of the (a) *S. horneri*, (b) HC and (c, d) KOH-activated carbon (AHC).

The peak at 1620 cm^{-1} corresponded to the C=C stretching vibration [52]. The absorption bands observed in the range of 1000–1450 cm^{-1} represented the C-O stretching vibrations [53]. The bands at 500–800 cm^{-1} region corresponded to out-of-plane N-H deformation vibration [34]. The characteristic peaks of HC were consistent with those of other biomass-based hydrochars [47]. Instead, as for AHC, only the weak O-H vibration band, C=C vibration band, and N-H deformation vibration were detected. The intensity of these characteristic peaks decreased dramatically due to the violent chemical reaction between HC and KOH. The abovementioned facts indicated that the CO_2 adsorption of HC could be assigned to chemisorption that resulted from the rich oxygen- and nitrogen-containing functional groups, whereas the adsorption of AHC would be determined by the relative pore structure and residual chemical functional groups.

The XRD patterns of HC and AHC are shown in Figure 6. The XRD pattern of the HC displayed a sharp diffraction peak around $2\theta = 22.5^{\circ}$, corresponding to the (002) interlayer reflection. However, almost no sharp (002) diffraction peak has been observed in the hydrochars from other biomass [54]. This phenomenon indicated that the formation of graphitic structures was promoted by hydrothermal treatment in the presence of metal catalysts. Compared to HC, the (002) diffraction pattern of AHC exhibited a broad diffraction peak at around 25° and a week diffraction band at around 43°, attributing to the (002) and (100) planes, respectively. The broad (002) diffraction peak indicated that the graphitization degree decreased since KOH activation destroyed the graphite layer of HC.

3.4. Porosity Formation of Activated Carbon. Several pathways of porosity formation in AHC are proposed and described schematically in Figure 7. Firstly, the intrinsic channel-like structure of *S. horneri* contributes to the formation of macropores. As observed in Figure 2(b), the cross-linked macroporous structure is obtained by hydrothermal carbonization of *S. horneri*. The unique structure is ascribed to the special structure and component of *S. horneri*, hydrothermal carbonization and catalyst. *S. horneri* is mainly composed of hemicellulose, cellulose and lignin. In a structural context, the cellulose in *S. horneri* is mainly cross linked with hemicellulose and lignin [55]. Hemicellulose is easy to liquefy and degrades into smaller molecules under mild hydrothermal temperature (180°C) [56], while the cellulose and lignin significantly decomposes under hydrothermal conditions above approximately 200°C [57, 58]. Accordingly, the cellulose and lignin can be selectively retained at around 180°C and form a solid scaffold with the cross-linked structure, contributing to the opening and linking channel.

Secondly, iron ion can accelerate hydrothermal carbonization reaction and promote the formation of pores. Cui et al. [37] reported that metal ions, such as iron ions, could effectively accelerate the hydrothermal carbonization process, which shortened the reaction time to some hours. Moreover, Braghiroli et al. [38] pointed out that the iron ion had a catalytic effect on the production of gas, contributing to the production of carbon materials with higher porosity and surface area. In our previous experiments, we explored the effects of the ammonium iron (II) sulfate hexahydrate in the HTC process and hydrochar. The results showed that the reaction time of hydrothermal carbonization was shortened

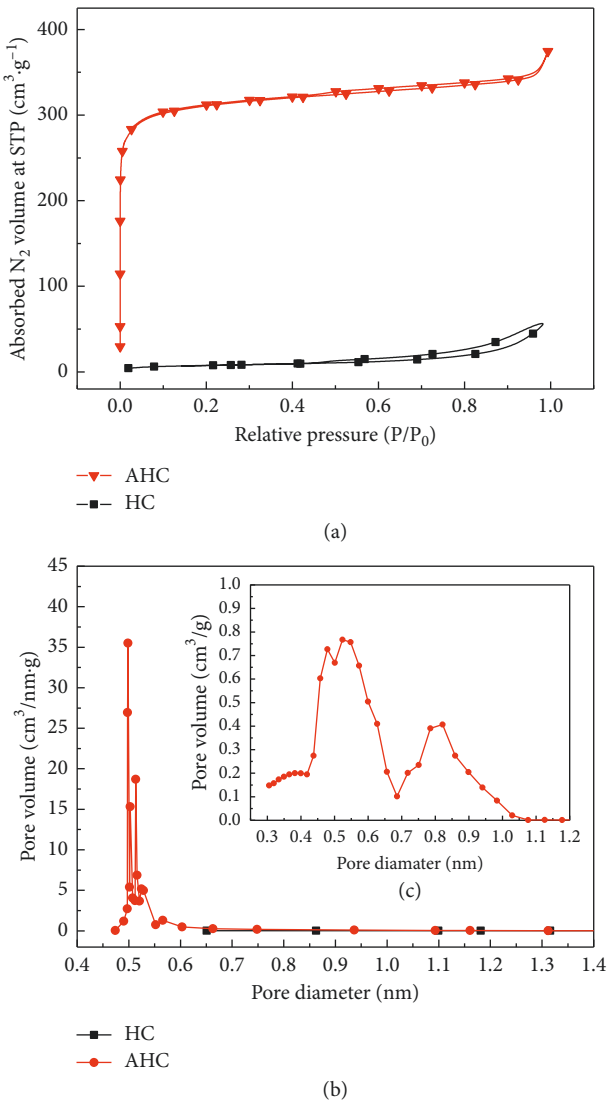

Figure 3: (a) N_2 sorption-desorption isotherms and corresponding pore size distributions derived from (b) N_2 adsorption and (c) CO_2 sorption.

Table 1: Textural properties of *S. horneri*-based carbon.

Sample	S_{BET} ($m^2 \cdot g^{-1}$)	V_{total} ($cm^3 \cdot g^{-1}$)	V_{micro} ($cm^3 \cdot g^{-1}$)	Average pore sizes (nm)
S. horneri	0.43	0.0051	0.00	21.77
HC	26.64	0.093	0.0007	13.96
AHC	1221	0.58	0.38	2.16

to 2 hours with the addition of catalyst in the HTC process; besides, the BET surface area and total volume of the hydrochar increased significantly.

Thirdly, KOH activation plays a vital role in pore evolution. A redox reaction has taken place during KOH activation, where the carbon is oxidized to CO or CO_2, thus generating pores [59]. The developed porosity can be achieved through adjusting the activation conditions [24]. Compared with HC, AHC exhibited higher specific surface area (1221 m^2/g), micropores volume (0.38 m^3/g), and narrower distributed micropores (~0.50 nm), indicating that the KOH activation contributes the most to the formation of micropore structures [60].

Finally, small gas molecules such as CO, CO_2, CH_4, and H_2O are released via carbon gasification during the activation process with the increasing temperature, facilitating the development of pores. The combination of four proposed porosity formation pathways well explains the structure of AHC with abundant micropores (~0.50 nm).

3.5. CO_2 Uptake Capacity. The CO_2 uptake capacities (q_e) of HC and AHC were studied at 30°C, 45°C, and 60°C. Although AHC had less nitrogen content, it showed higher CO_2 adsorption capacities of 101.7, 92, and 54 mg/g than HC at 30°C, 45°C, and 60°C and 1 bar, as shown in Table 3. This is due to the fact that the CO_2 uptake of activated carbon was not only contributed by functional groups on the surface, but also determined by the porous structure and specific surface area [61]. Though HC had more functional groups, the further CO_2 adsorption was limited as a consequence of its low porosity and negligible micropore volume. AHC exhibited a developed pore structure, such as high specific surface area and microporous volume. As shown in Table 1, the significant increase in micropore volume of AHC compared to HC indicates that the activation process primarily enhanced the CO_2 physical adsorption. Therefore, HC exhibited that certain CO_2 sorption capacity was mostly due to its functional groups on the external surface, while CO_2 adsorption on AHC was primarily attributed to abundant narrow micropores (~0.50 nm).

AHC exhibited CO_2 adsorption capacity as high as 101.7 mg/g at 30°C and decreased to 92 mg/g at 45°C and 54 mg/g at 60°C, respectively, caused by the exothermic nature of adsorption. In addition, AHC had a considerable CO_2 adsorption capacity over other carbon materials as shown in Table 4. As a result, AHC was produced from marine waste via a facile method and was used as a CO_2 adsorbent, alleviating the *S. horneri* golden tides.

3.6. Adsorption Kinetic. To assess the CO_2 adsorption kinetic, the CO_2 adsorption on AHC was conducted by TGA at 30°C under atmospheric pressure. The pseudo-first-order and pseudo-second-order models were used to fit the isotherm of AHC. The pseudo-first-order equation is applied to determine the kinetic parameters:

$$q_t = q_e\left(1 - e^{-k_1 t}\right), \quad (1)$$

where q_t and q_e ($mg \cdot g^{-1}$) are the adsorption capacities at time t (min) and at equilibrium, respectively, and k_1 (min^{-1}) is the kinetic rate constant of the pseudo-first-order kinetic model.

The pseudo-second-order equation is expressed as follows:

$$q_t = \frac{q_e^2 k_2 t}{1 + q_e k_2 t}, \quad (2)$$

where k_2 ($mg \cdot min^{-1}$) is the rate constant of second-order-adsorption.

Table 2: Elemental analysis of *S. horneri*, HC, and AHC.

Samples	C (wt.%)	H (wt.%)	N (wt.%)	S (wt.%)	O*(wt.%)	H/C (atomic ratio)	O/C (atomic ratio)
S. horneri	41.25	5.70	3.43	0.68	48.94	1.66	0.89
HC	52.77	4.95	4.32	0.27	37.69	1.13	0.54
AHC	71.40	2.65	3.56	0.29	22.10	0.44	0.23

*Calculated by the difference.

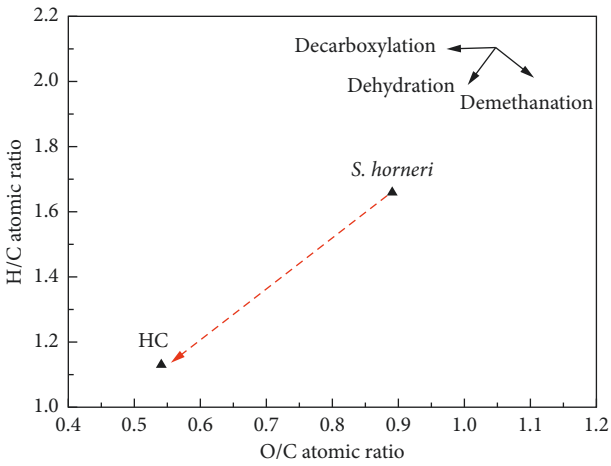

Figure 4: Van Krevelen diagram for *S. horneri* and its hydrochar.

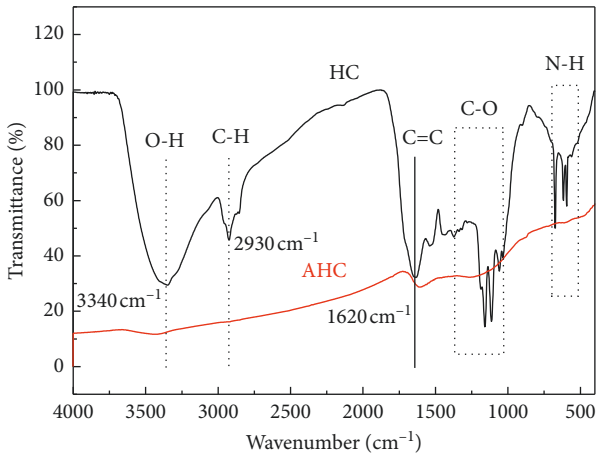

Figure 5: FTIR spectra of HC and AHC.

Figure 8 showed experimental CO_2 uptake as a function of time on the AHC and the corresponding profiles obtained from the two adsorption kinetic models. Table 5 summarizes the related parameters of kinetic models. It was observed that the pseudo-first-order model gave a better fit than the pseudo-second-order model with the experimental data for CO_2 adsorption on the AHC. This was further confirmed by higher R^2 and lower error % values. Thus, the pseudo-first-order kinetic model provided a better description over the entire adsorption process. It showed two stages: in the first stage, approximately 70% of the total CO_2 uptake reached within 6 min, and the adsorption process for the second stage was slow. This behavior could be attributed to the decreased unoccupied active

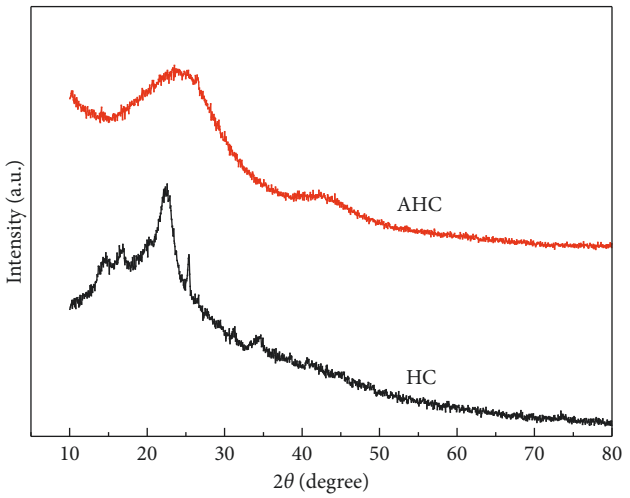

Figure 6: XRD patterns of HC and AHC.

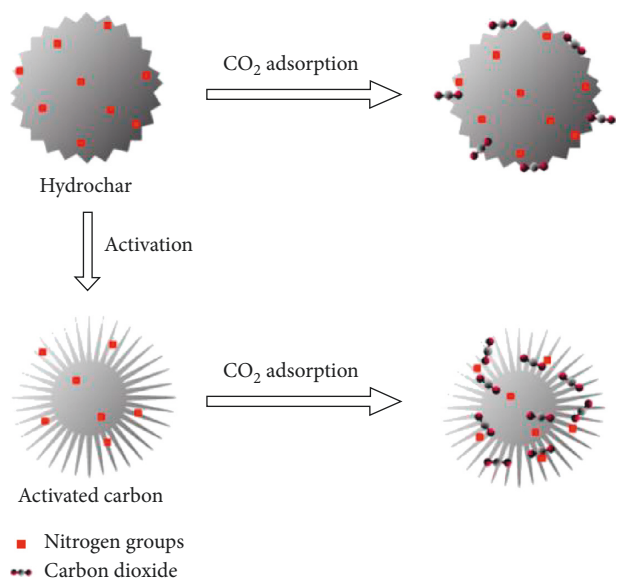

Figure 7: Schematic diagram of the porosity formation of AHC.

Table 3: CO_2 equilibrium adsorption capacities of carbon materials at different temperatures.

Sample	CO_2 uptake-100% CO_2/mg·g^{-1} (mmol·g^{-1})		
	30°C	45°C	60°C
HC	36 (0.8)	23 (0.5)	17 (0.4)
AHC	101.7 (2.3)	92 (2.1)	54 (1.2)

Table 4: Comparisons of adsorbent capacity.

Sorbent	Temperature (K)	CO_2 uptake/mg·g^{-1} (mmol·g^{1})	Reference
Enteromorpha prolifera-based activated carbon	298	61 (1.4)	[34]
Mesoporous sucrose-based activated carbon	298	76 (1.7)	[62]
Amino-modified peat-based activated carbon	298	96 (2.2)	[63]
A material composed by zeolite and activated carbon	298	116 (2.63)	[64]
A metal-rich wood-based activated carbon	298	83 (1.9)	[65]
Waste ion-exchange resin-based activated carbon	303	81.2 (1.8)	[66]
Sargassum horneri-based porous carbon (AHC)	303	101.7 (2.3)	This work

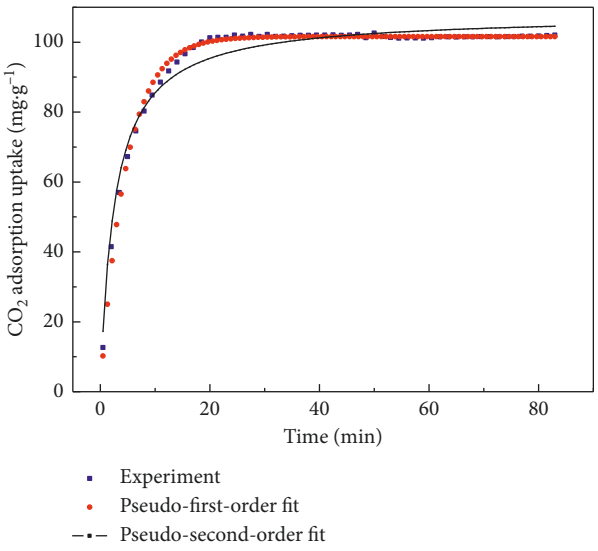

Figure 8: Experimental CO_2 uptake on AHC and corresponding fit to kinetic models at 30°C.

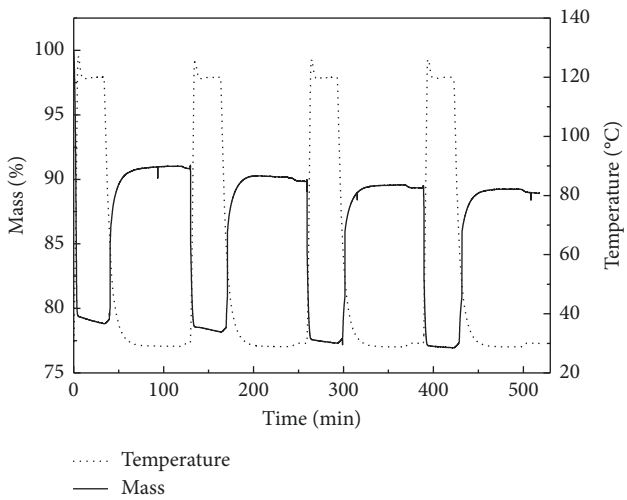

Figure 9: CO_2 adsorption-desorption cycles obtained for the AHC at 30°C (CO_2 concentration: 100%).

Table 5: The kinetic parameters of CO_2 adsorption on activated carbon.

Kinetic models	Kinetic parameters			
	q_e (mg·g^{-1})	k	R^2	Error (%)
Pseudo-first-order kinetic	101.6	0.21205 (min^{-1})	0.99218	3.57
Pseudo-second-order kinetic	107.8	0.00355 (mg·min^{-1})	0.96796	6.09

sites and the increased diffusion resistance [67]. The above facts illustrated that AHC had a rapid CO_2 adsorption rate, which was beneficial for industrial application.

3.7. Adsorbent Regeneration. Except for high CO_2 adsorption capacity, cyclic stability and ease of regeneration were also important criterions for efficient CO_2 capture in practical applications. A cyclic test was performed by alternatively repeating adsorption-desorption cycles at 30°C and 1 bar, as shown in Figure 9. It can be seen that the adsorbed CO_2 was easily desorbed by purging with N_2. Actually, more than 94% of CO_2 could be desorbed within 3 min under desorption conditions. Besides, no noticeable changes in the CO_2 adsorption capacity were observed after four successive cycles of adsorption-desorption. Thus, the AHC could be successfully regenerated at 30°C and 1 bar and showed highly cyclic stability with ~99% of the initial adsorption capacity over multiple cycles, which is highly desirable for potential industrial applications.

4. Conclusion

In summary, we reported a facile method for preparing microporous carbon from *S. horneri* via the hydrothermal carbonization and subsequent KOH activation, which shortens the hydrothermal reaction time and the dosage of the activating agent. It was found that the hydrothermal carbonization of *S. horneri* at 180°C for 2 h is a suitable condition for the production of HC with high yield and macroporous structure. AHC with abundant microporous structure (~0.50 nm) has been synthesized using a KOH/HC ratio of 1 at 600°C. Then, the CO_2 uptake of HC and AHC has been studied under different temperatures. The result illustrated that AHC is more suitable as a CO_2 adsorbent, and the low adsorption temperature facilitates the CO_2 uptake. The high CO_2 uptake of 101.7 mg/g has been achieved using AHC at 30°C. The high CO_2 uptake is primarily ascribable to the presence of abundant narrow micropores (~0.50 nm). Moreover, the AHC exhibits a rapid CO_2 adsorption rate, excellent cyclic stability, and easy regeneration. As such, marine waste, *S. horneri* can serve as a potential raw material for developing a high-performance and cost-effective CO_2

adsorbent. Our study also provides a feasible approach to alleviate the golden tides caused by macroalgae.

Data Availability

The data used to support the findings of this study are included within the article.

Conflicts of Interest

The authors declare no conflicts of interest.

Acknowledgments

This work was supported by the National Natural Science Foundation of China (grant nos. 21628601 and 51728902), the Zhejiang Provincial Natural Science Foundation of China (grant nos. LY16B060014 and LGF18D060002), and the State Key Laboratory of Chemical Engineering (no. SKL-ChE-08A01).

References

[1] K. G. Collins, G. F. Fitzgerald, C. Stanton, and R. P. Ross, "Looking beyond the terrestrial: the potential of seaweed derived bioactives to treat non-communicable diseases," *Marine Drugs*, vol. 14, no. 3, p. 60, 2016.

[2] M. B. Ariede, T. M. Candido, A. L. M. Jacome, M. V. R. Velascoa, J. C. M. Carvalho, and A. R. Baby, "Cosmetic attributes of algae—a review," *Algal Research*, vol. 25, pp. 483–487, 2017.

[3] K. Sudhakar, R. Mamat, M. Samykano, W. H. Azmi, W. F. W. Ishak, and T. Yusaf, "An overview of marine macroalgae as bioresource," *Renewable and Sustainable Energy Reviews*, vol. 91, pp. 165–179, 2018.

[4] T. Komatsu, K. Tatsukawa, J. B. Filippi et al., "Distribution of drifting seaweeds in eastern East China Sea," *Journal of Marine Systems*, vol. 67, no. 3-4, pp. 245–252, 2007.

[5] V. Smetacek and A. Zingone, "Green and golden seaweed tides on the rise," *Nature*, vol. 504, no. 7478, pp. 84–88, 2013.

[6] Q. G. Xing, R. H. Guo, L. L. Wu et al., "High-resolution satellite observations of a new hazard of golden tides caused by floating *Sargassum* in winter in the Yellow Sea," *IEEE Geoscience and Remote Sensing Letters*, vol. 14, no. 10, pp. 1815–1819, 2017.

[7] C. Zhao, C. Yang, B. Liu et al., "Bioactive compounds from marine macroalgae and their hypoglycemic benefits," *Trends in Food Science and Technology*, vol. 72, pp. 1–12, 2017.

[8] H. P. S. A. Khalil, T. K. Lai, Y. Y. Tye et al., "A review of extractions of seaweed hydrocolloids: properties and applications," *Express Polymer Letters*, vol. 12, no. 4, pp. 296–317, 2018.

[9] I. Biancarosa, N. S. Liland, D. Biemans et al., "Uptake of heavy metals and arsenic in black soldier fly (*Hermetia illucens*) larvae grown on seaweed-enriched media," *Journal of the Science of Food and Agriculture*, vol. 98, no. 6, pp. 2176–2183, 2018.

[10] J. Jegan, J. Vijayaraghavan, T. Bhagavathi Pushpa, and S. J. Sardhar Basha, "Application of seaweeds for the removal of cationic dye from aqueous solution," *Desalination and Water Treatment*, vol. 57, no. 53, pp. 25812–2582, 2016.

[11] S. O. Lourenc, E. Barbarino, J. C. De-Paula, L. O. D. S. Pereira, and U. M. L. Marquez, "Amino acid composition, protein content and calculation of nitrogen-to-protein conversion factors for 19 tropical seaweeds," *Phycological Research*, vol. 50, no. 3, pp. 233–241, 2002.

[12] W. Zhao, P. Yuan, X. She et al., "Sustainable seaweed-based one-dimensional (1D) nanofibers as high-performance electrocatalysts for fuel cells," *Journal of Materials Chemistry A*, vol. 3, no. 27, pp. 14188–14194, 2015.

[13] L. Hencz, X. Gu, X. Zhou, W. Martens, and S. Zhang, "Highly porous nitrogen-doped seaweed carbon for high-performance lithium-sulfur batteries," *Journal of Materials Science*, vol. 52, no. 20, pp. 12336–12347, 2017.

[14] M. Sevilla, W. Gu, C. Falco, M. M. Titirici, A. B. Fuertes, and G. Yushin, "Hydrothermal synthesis of microalgae-derived microporous carbons for electrochemical capacitors," *Journal of Power Sources*, vol. 267, pp. 26–32, 2014.

[15] F. Shen, Y. Wang, L. Y. Li, K. Q. Zhang, R. L. Smith, and X. H. Qi, "Porous carbonaceous materials from hydrothermal carbonization and KOH activation of corn stover for highly efficient CO_2 capture," *Chemical Engineering Communications*, vol. 205, no. 4, pp. 423–431, 2018.

[16] H. S. Kambo and A. Dutta, "A comparative review of biochar and hydrochar in terms of production, physic-chemical properties and applications," *Renewable and Sustainable Energy Reviews*, vol. 45, pp. 359–378, 2015.

[17] M. M. Titirici and M. Antonietti, "Chemistry and materials options of sustainable carbon materials made by hydrothermal carbonization," *Chemical Society Reviews*, vol. 39, no. 1, pp. 103–116, 2010.

[18] Q. H. Lin, H. Cheng, and G. Y. Chen, "Preparation and characterization of carbonaceous adsorbents from sewage sludge using a pilot-scale microwave heating equipment," *Journal of Analytical and Applied Pyrolysis*, vol. 93, pp. 113–119, 2012.

[19] V. Jiménez, A. Ramírez-Lucas, J. A. Díaz, and A. Romero, "CO_2 capture in different carbon materials," *Environmental Science & Technology*, vol. 46, no. 13, pp. 7407–7414, 2012.

[20] N. P. Wickramaratne and M. Jaroniec, "Importance of small micropores in CO_2 capture by phenolic resin-based activated carbon spheres," *Journal of Materials Chemistry A*, vol. 1, no. 1, pp. 112–116, 2013.

[21] M. Sevilla and A. B. Fuertes, "Sustainable porous carbons with a superior performance for CO_2 capture," *Energy & Environmental Science*, vol. 4, no. 5, pp. 1765–1771, 2011.

[22] V. Presser, J. Mcdonough, S. H. Yeon, and Y. Gogotsi, "Effect of pore size on carbon dioxide sorption by carbide derived carbon," *Energy & Environmental Science*, vol. 4, no. 8, pp. 3059–3066, 2011.

[23] Z. S. Zhang, J. Zhou, W. Xing et al., "Critical role of small micropores in high CO_2 uptake," *Physical Chemistry Chemical Physics*, vol. 15, no. 7, pp. 2523–2529, 2013.

[24] M. Sevilla, J. B. Parra, and A. B. Fuertes, "Assessment of the role of micropore size and N-doping in CO_2 capture by porous carbons," *ACS Applied Materials & Interfaces*, vol. 5, no. 13, pp. 6360–6368, 2013.

[25] L. W. Wang, L. L. Rao, B. B. Xia et al., "Highly efficient CO_2 adsorption by nitrogen-doped porous carbons synthesized with low-temperature sodium amide activation," *Carbon*, vol. 130, pp. 31–40, 2018.

[26] Y. Zhao, X. Liu, K. X. Yao, L. Zhao, and Y. Han, "Superior capture of CO_2 achieved by introducing extra-framework cations into N-doped microporous carbon," *Chemistry of Materials*, vol. 24, no. 24, pp. 4725–4734, 2012.

[27] A. D. Roberts, J. S. M. Lee, S. Y. Wong, X. Li, and H. Zhang, "Nitrogen-rich activated carbon monoliths via ice-templating

with high CO_2 and H_2 adsorption capacities," *Journal of Materials Chemistry A*, vol. 5, no. 6, pp. 2811–2820, 2017.

[28] H. Gan, J. Cai, C. Zhang, Z. Dong, H. Jin, and K. Zhang, "Coadsorption of antibiotic amoxicillin and hexavalent chromium from saline water by seaweed-based porous activated carbon," *Desalination and Water Treatment*, vol. 67, pp. 389–396, 2017.

[29] M. J. Pintor, C. Jean-Marius, V. Jeanne-Rose et al., "Preparation of activated carbon from *Turbinaria turbinata* seaweeds and its use as supercapacitor electrode materials," *Comptes Rendus Chimie*, vol. 16, no. 1, pp. 73–79, 2013.

[30] S. E. M. Pourhosseini, O. Norouzi, and H. R. Naderi, "Study of micro/macro ordered porous carbon with olive-shaped structure derived from *Cladophora glomerata*, macroalgae as efficient working electrodes of supercapacitors," *Biomass and Bioenergy*, vol. 107, pp. 287–298, 2017.

[31] X. Wu, Z. Tian, L. Hu, S. Huang, and J. Cai, "Macroalgae-derived nitrogen-doped hierarchical porous carbons with high performance for H_2 storage and supercapacitors," *RSC Advances*, vol. 7, no. 52, pp. 32795–32805, 2017.

[32] F. Liu, L. Liu, X. Li, J. Zeng, L. Du, and S. Liao, "Nitrogen self-doped carbon nanoparticles derived from spiral seaweeds for oxygen reduction reaction," *RSC Advances*, vol. 6, no. 33, pp. 27535–27541, 2016.

[33] B. Escobar, K. Y. Pérez-Salcedo, I. L. Alonso-Lemus, D. Pacheco, and R. Barbosa, "N-doped porous carbon from Sargassum, spp. as metal-free electrocatalysts for oxygen reduction reaction in alkaline media," *International Journal of Hydrogen Energy*, vol. 42, no. 51, pp. 30274–30283, 2017.

[34] Z. Q. Zhang, K. Wang, J. D. Atkinson et al., "Sustainable and hierarchical porous *Enteromorpha prolifera* based carbon for CO_2 capture," *Journal of Hazardous Materials*, vol. 229-230, pp. 183–191, 2012.

[35] G. N. Zeng, X. WU, N. AI, J. W. Wang, M. L. Tu, and H. Y. Zhou, "Hydrothermal preparation and characterization of biochar from *Sargassum Horneri*," *Acta Scientiae Circumstantiae*, vol. 34, pp. 392–397, 2014.

[36] Q. Xu, Q. Qian, A. Quek, N. Ai, G. Zeng, and J. W. Wang, "Hydrothermal carbonization of macroalgae and the effects of experimental parameters on the properties of hydrochars," *ACS Sustainable Chemistry & Engineering*, vol. 1, no. 9, pp. 1092–1101, 2013.

[37] X. Cui, M. Antonietti, and S. H. Yu, "Structural effects of iron oxide nanoparticles and iron ions on the hydrothermal carbonization of starch and rice carbohydrates," *Small*, vol. 2, no. 6, pp. 756–759, 2010.

[38] F. L. Braghiroli, V. Fierro, A. Szczurek et al., "Hydrothermal treatment of tannin: a route to porous metal oxides and metal/carbon hybrid materials," *Inorganics*, vol. 5, no. 1, p. 7, 2017.

[39] M. M. Titirici, A. Thomas, S. H. Yu, J. O. Müller, and M. Antonietti, "A direct synthesis of mesoporous carbons with bicontinuous pore morphology from crude plant material by hydrothermal carbonization," *Chemistry of Materials*, vol. 19, no. 17, pp. 4205–4212, 2007.

[40] Z. Y. Li, X. Y. Gao, L. Wu, K. W. Wang, and N. Kobayashi, "Preparation of activated carbons from poplar wood by chemical activation with KOH," *Journal of Porous Materials*, vol. 24, no. 1, pp. 193–202, 2017.

[41] S. S. Kim, H. V. Ly, J. Kim, J. H. Choi, and H. C. Woo, "Thermogravimetric characteristics and pyrolysis kinetics of alga sagarssum sp. biomass," *Bioresource Technology*, vol. 139, pp. 242–248, 2013.

[42] D. Li, L. Chen, X. Zhang, N. Ye, and F. Xing, "Pyrolytic characteristics and kinetic studies of three kinds of red algae," *Biomass and Bioenergy*, vol. 35, no. 5, pp. 1765–1772, 2011.

[43] Y. Wei, J. J. Hong, and W. R. Ji, "Thermal characterization and pyrolysis of digestate for phenol production," *Fuel*, vol. 232, pp. 141–146, 2018.

[44] P. Gao, Y. Y. Zhou, F. Meng et al., "Preparation and characterization of hydrochar from waste eucalyptus bark by hydrothermal carbonization," *Energy*, vol. 97, pp. 238–245, 2016.

[45] L. Luo, T. Chen, Z. Li, Z. Zhang, W. Zhao, and M. Fan, "Heteroatom self-doped activated biocarbons from fir bark and their excellent performance for carbon dioxide adsorption," *Journal of CO_2 Utilization*, vol. 25, pp. 89–98, 2018.

[46] H. Zhou, J. Zhang, I. S. Amiinu et al., "Transforming waste biomass with an intrinsically porous network structure into porous nitrogen-doped graphene for highly efficient oxygen reduction," *Physical Chemistry Chemical Physics*, vol. 18, no. 15, pp. 10392–10399, 2016.

[47] J. Mumme, L. Eckervogt, J. Pielert, M. Diakité, F. Rupp, and J. Kern, "Hydrothermal carbonization of anaerobically digested maize silage," *Bioresource Technology*, vol. 102, no. 19, pp. 9255–9260, 2011.

[48] Z. Liu, F. S. Zhang, and J. Wu, "Characterization and application of chars produced from pinewood pyrolysis and hydrothermal treatment," *Fuel*, vol. 89, no. 2, pp. 510–514, 2010.

[49] X. J. Cui, R. M. Bustin, and G. Dipple, "Selective transport of CO_2, CH_4, and N_2 in coals: insights from modeling," *Fuel*, vol. 83, no. 3, pp. 293–303, 2004.

[50] D. W. V. Krevelen, "Graphical statistical method for the study of structure and reaction processes of coal," *Fuel*, vol. 29, pp. 269–284, 1950.

[51] X. T. Zhang, J. Zhang, W. H. Song, Z. F. Song, and Z. F. Liu, "Controllable synthesis of conducting polypyrrole nanostructures," *Journal of Physical Chemistry B*, vol. 110, no. 3, pp. 1158–1165, 2006.

[52] S. W. Hao, C. H. Hsu, Y. G. Liu, and B. K. Chang, "Activated carbon derived from hydrothermal treatment of sucrose and its air filtration application," *RSC Advances*, vol. 6, no. 111, pp. 109950–109959, 2016.

[53] M. Sevilla and A. B. Fuertes, "The production of carbon materials by hydrothermal carbonization of cellulose," *Carbon*, vol. 47, no. 9, pp. 2281–2289, 2009.

[54] M. D. Demir, Z. K. Kahveci, B. Aksoy et al., "Graphitic biocarbon from metal-catalyzed hydrothermal carbonization of lignin," *Industrial & Engineering Chemistry Research*, vol. 54, no. 43, pp. 10731–10739, 2015.

[55] N. Syaftika and Y. Matsumura, "Comparative study of hydrothermal pretreatment for rice straw and its corresponding mixture of cellulose, xylan, and lignin," *Bioresource Technology*, vol. 255, pp. 1–6, 2018.

[56] O. Bobleter, "Hydrothermal degradation of polymers derived from plants," *Progress in Polymer Science*, vol. 19, no. 5, pp. 797–841, 1994.

[57] C. R. Correa and A. Kruse, "Biobased functional carbon materials: production, characterization, and applications—a review," *Materials*, vol. 11, no. 9, p. 1568, 2018.

[58] A. Funke and F. Ziegler, "Hydrothermal carbonization of biomass: a summary and discussion of chemical mechanisms for process engineering," *Biofuels Bioproducts and Biorefining*, vol. 4, no. 2, pp. 160–177, 2010.

[59] M. Molina-Sabio and F. Rodriguez-Reinoso, "Role of chemical activation in the development of carbon porosity,"

Colloids and Surfaces A: Physicochemical and Engineering Aspects, vol. 241, no. 1–3, pp. 15–25, 2004.

[60] A. S. Ello, L. K. C. D. Souza, A. Trokourey, and M. Jaroniec, "Development of microporous carbons for CO_2 capture by KOH activation of African palm shells," *Journal of CO_2 Utilization*, vol. 2, pp. 35–38, 2013.

[61] W. Z. Shen, S. C. Zhang, Y. He, J. F. Li, and W. B. Fan, "Hierarchical porous polyacrylonitrile-based activated carbon fibers for CO_2 capture," *Journal of Materials Chemistry*, vol. 21, no. 36, pp. 14036–14040, 2011.

[62] G. Chandrasekar, W. J. Son, and W. S. Ahn, "Synthesis of mesoporous materials SBA-15 and CMK-3 from fly ash and their application for CO_2 adsorption," *Journal of Porous Materials*, vol. 16, no. 5, pp. 545–551, 2009.

[63] M. S. Shafeeyan, W. M. A. W. Daud, A. Houshmand, and A. Arami-Niya, "Ammonia modification of activated carbon to enhance carbon dioxide adsorption: effect of pre-oxidation," *Applied Surface Science*, vol. 257, no. 9, pp. 3936–3942, 2011.

[64] M. J. Regufe, A. F. P. Ferreira, J. M. Loureiro, Y. X. Shi, A. Rodrigues, and A. M. Ribeiro, "New hybrid composite honeycomb monolith with 13X zeolite and activated carbon for CO_2 capture," *Adsorption*, vol. 24, no. 3, pp. 249–265, 2018.

[65] M. L. Botomé, P. Poletto, J. Junges, D. Perondi, A. Dettmer, and M. Godinho, "Preparation and characterization of a metal-rich activated carbon from CCA-treated wood for CO_2 capture," *Chemical Engineering Journal*, vol. 321, pp. 614–621, 2017.

[66] M. Q. Wei, Q. B. Yu, T. Mu, L. M. Hou, Z. L. Zuo, and J. Y. Peng, "Preparation and characterization of waste ion-exchange resin-based activated carbon for CO_2 capture," *Adsorption*, vol. 22, no. 3, pp. 385–396, 2016.

[67] D. Tiwari, H. Bhunia, and P. K. Bajpai, "Development of chemically activated N-enriched carbon adsorbents from urea-formaldehyde resin for CO2 adsorption: kinetics, isotherm, and thermodynamics," *Journal of Environmental Management*, vol. 218, pp. 579–592, 2018.